Structure estimation of 2D listric faults using quadratic Bezier curve for depth varying density distributions

Arka Roy[1,2], Thatikonda Suresh Kumar[1], Rajat Kumar Sharma,[1]

[1]National Centre for Earth Science Studies, Akkulam, Trivandrum, Kerala, India - 695011.
[2]Cochin University of Science and Technology, Kochi, Kerala, India - 682022.

Key Points:

- Listric fault inversion from observed gravity anomalies
- Fault plane parametrization using Bezier curve and optimization using PSO
- Graphical User interface for inverting real fault structures

Corresponding author: Arka Roy, arka.phy@gmail.com

Abstract

A contemporary and decisive optimization algorithm is developed for inverting gravity anomalies due to listric faults. The cross-section of listric faults are generally concave up, and the dip of the fault plane gradually decreases with depth. Quadratic Bezier curves are utilized to represent the curvature of the fault plane. The densities of sediment deposition are assumed to be known and can take any functional form of depth. By constraining the density, a global optimization algorithm is adopted to estimate the fault structure by inverting control point parameters of Bezier curves. The presented algorithm is implemented in two different synthetic models having fixed and depth varying density contrasts. The robustness of the algorithm is authenticated by incorporating white Gaussian noise into synthetic gravity anomalies. A detailed uncertainty appraisal is also performed to justify the reliability of the algorithm. Finally, a real structure is reconstructed using observed gravity anomalies, and the estimated structure is verified with the structure obtained in previously published literature. Furthermore, a Matlab based GUI is developed such that any user can estimate real listric fault structure without any computational difficulties.

1 Introduction

Listric faults were first introduced by Suess (1909) for describing faults in coal mines in northern France. The fault planes of listric faults are generally upward concave in nature, and the dip decreases with depth (Shelton, 1984). Listric faults have particular importance in the formation of sedimentary basins. Most of the listric faults are generally occurs during the formation of rift or formation of passive continental margins (Bally et al., 1981). The curvature occurred due to the thick sediment depositions in case of boundary faults (Chakravarthi, 2011). Listric fault can produce structural trap by relative displacement of strata to create a barrier to petroleum migration (Sheth, 1998; Yamada & McClay, 2003). It also has structural importance for mineral explorations (Song et al., 2012). The gravity method is one of the oldest geophysical approaches for subsurface imaging. In general, gravity inversion for subsurface parameter estimation is non-unique but by incorporating proper constraints (Y. Li & Oldenburg, 1996; Portniaguine & Zhdanov, 2002) a stable and converging parameter optimization can be achieved. In our present study, the density contrast is assumed to be known from borehole logging and used as a constraint for fault structure estimation. Furthermore, an uncertainty appraisal provides a reliable solution for any ill-posed problem.

The gravity method is one of the passive geophysical techniques to study the interior of the Earth. The ground gravity survey is very fast, inexpensive, and can cover a large study area via non-destructive measurements. The gravity method plays a vital role in geological structure estimation and exploration purposes. There are numerous implementations, such as, structure estimation of sedimentary basins (Silva et al., 2006; Zhou, 2013; Pallero et al., 2015; A. Roy et al., 2021b), faults and folds (L. Roy et al., 2000; Chakravarthi & Sundararajan, 2004, 2007b; A. Roy & Kumar, 2021) due to crustal deformations, glaciology (Crossley & Clarke, 1970; Tinto & Bell, 2011) and hydro-geology (Alatorre-Zamora & Campos-Enriquez, 1991; Güntner et al., 2007) etc. The exploration study includes mining (Jaffal et al., 2010; Veiga & Gunson, 2020), hydrocarbon exploration (Rose et al., 2006; W. Li et al., 2016), cavity detection etc. The gravitational inversion is a useful tool to interpret the gravity data for subsurface imaging. Density and corresponding geometries of the subsurface structure are the two parameters for geophysical optimization using gravity anomalies. Optimization algorithms are referred to a mathematical procedure for finding parameters by minimizing the objective function. As per the algorithms' demand, one can categorize optimization algorithms as (1) algorithms that use derivative information, (2) algorithms that do not require derivative information of objective function. Here are a few examples of optimization algorithms that require derivative information for gravity inversion. Chakravarthi and Sundararajan (2007a, 2007b) used Marquardt optimization for structure estimation using gravity anomalies, Silva et al. (2014) developed a fast inversion

technique using Gauss-Newton optimization for inverting basement relief. Florio (2020) used iterative rescaling approach for evaluating 3D basement depth. Qin et al. (2016) inverted 3D gravity anomalies using a non-linear conjugate gradient optimization algorithm. X. Feng et al. (2018) derived a combined multinorm and normalized vertical derivative technique for 3D gravity inversion of basement relief. Most of the global optimization algorithm does not require any derivative information as well as any pre-requisite models. Such algorithms are mainly population-based and use iterative schemes for optimization. Some of the examples of population-based algorithms that used in gravity inversion are differential evolution (Ekinci et al., 2016; A. Roy et al., 2021a), genetic algorithm (Zhang et al., 2004; Montesinos et al., 2005), very fast simulated annealing (Nagihara & Hall, 2001; Biswas, 2015), ant colony optimization (Srivastava et al., 2014), particle swarm optimization (Pallero et al., 2015; Essa & Munschy, 2019) etc. Particle swarm optimization is one of the most popular global optimization schemes due to its simple architecture, easy implementation and computational efficiency. Here we adapted PSO for optimizing listric fault structures from observed gravity anomalies.

Several authors performed an extensive study for inverting planner faults by different optimization techniques. Due to the fault structure's geological importance, a continuous improvement of optimization algorithms is carried out for an accurate and fast converging structure estimation. In this direction Chakravarthi and Sundararajan (2004) derived an analytic ridge regression optimization technique for inclined fault inversion. Abdelrahman and Essa (2015) developed a least-square optimization, Essa (2013) performed a variance analysis method, Toushmalani (2013); Elhussein (2021) adopted PSO for dipping fault structure estimation having constant densities. In general, density can vary with depth for different types of sediment depositions, and incorporating variable density contrasts into models can provide accurate estimations. Minimal studies have been performed for inverting the listric fault plane from observed gravity anomalies. An automatic 2.5D listric fault inversion technique was developed by (Chakravarthi, 2011) for prescribed depth varying density contrasts. Further (Chakravarthi, 2010; Chakravarthi et al., 2017) characterized the fault plane in terms of higher-order polynomials for depth varying density distributions. In our present study, the listric fault planes are expressed using a quadratic Bezier curve for inverting gravity anomalies and estimating the underneath fault structure. The new algorithm can invert the listric fault plane for any depth varying density distributions without any prior initial model requirements. It is the first time developing such an algorithm for optimizing the listric fault plane using a quadratic Bezier curve with fewer parameter requirements.

2 Materials and Methods

This section illustrates the mathematical formulation for evaluating gravity anomalies due to any irregular inhomogeneous 2D structures. The Newtonian potential is the foundation for any potential theories, and we consider it for estimating gravity anomalies due to underneath anomalous densities. Various analytical simplifications and numerical techniques were developed for the faster and accurate computations of the potential field for irregular geometries. Finally, we implement it for forward modelling of listric faults having depth varying density distribution.

2.1 Forward Modelling

Forward modelling is the nitty-gritty for any global optimization problem. A forward model needs to be evaluated repeatedly during the inversion process for parameter estimation. Hence an inexpensive and less complex but meticulous forward model is always desirable for any faster converging optimization problem. In figure 1, a 2D irregular geometry having anomalous density is shown, for which the gravity anomaly has to be obtained at any observation point P (x_i, z_i). A convex polygon can approximate any irregular 2D shape (Talwani et al., 1959; Zhou, 2008, 2009; Wan & Zhang, 2019), and by increasing

the vertices of the polygon, it can more accurately mimic the original shape. Further, the vertical component of gravity anomaly (g_z) due to this strike infinite (y directional infinite extension) approximated 2D polygonal shape having density contrast $\Delta\rho$ can be estimated as a surface integral (Talwani et al., 1959) form

$$g_z(x_i, z_i) = 2G \iint_S \frac{\Delta\rho \cdot (z - z_i)}{(x - x_i)^2 + (z - z_i)^2}\, dx\, dz, \tag{1}$$

Where G is the universal gravitational constant. The density can vary anomalously in the horizontal and vertical directions. However, in our present study, we consider only depth varying density distribution $\Delta\rho(z)$, having any functional form of z. Using Stokes' theorem, the 2D area integral of irregular shape having depth varying density contrast can be converted into a line integral as

$$g_z(x_i, z_i) = -2G \oint_S \Delta\rho \cdot \arctan\left(\frac{x - x_i}{z - z_i}\right) dz \tag{2}$$

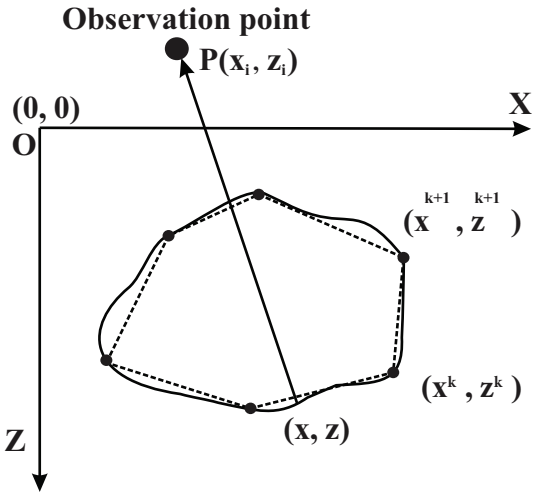

Figure 1. Polygon approximation of 2D irregular structure. The solid line represents the real mass source, and the dotted line represents approximated model.

The line integral can be numerically evaluated using Gauss Legendre quadrature formulation (Winckel, 2004). Let us assume the 2D irregular structure is approximated using a polygon (Figure 1) having N vertices, where (x^k, z^k) and (x^{k+1}, z^{k+1}) are two consecutive vertices. Hence the vertical component of gravity anomaly at any surface point P (x_i, z_i) due to the anomalous contrast $\Delta\rho(z)$ is expressed as

$$g_z(x_i, z_i) = -2G \sum_{k=1}^{N-1} \int_{z_k}^{z_{k+1}} \Delta\rho(z) \cdot \arctan\left(\frac{x - x_i}{z - z_i}\right) dz \tag{3}$$

In our present study, the prime objective is to invert gravity anomalies for inverting listric fault structure, and forward modelling of listric fault is an essential step for optimization. In figure 2, a generic architecture of the listric fault is shown, and the structure can be expressed by a polygon having four vertex points. In table 1, the locations of vertex

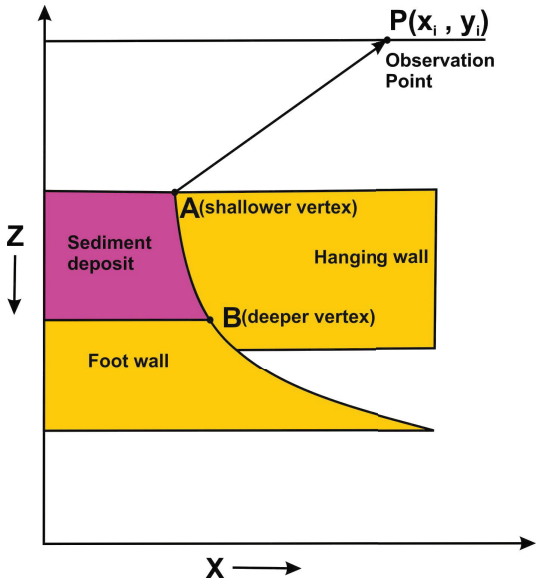

Figure 2. Generic representation of listric fault structure. AB represents the fault plane, and P is the observation point for estimating gravity anomalies.

points are given as per the orientation of the fault plane. Finally, the curvature of the listric fault plane is obtained using the quadratic Bezier curve. Hence, with the help of those four vertex points and locations of the fault plane from the Bezier curve, the forward model of any listric fault can be approximated. The vertical component of gravity anomaly can be estimated from the numerical line integral formulation using Gauss Legendre quadrature.

Table 1. Vertex locations for any generalized listric fault plane.

Vertex count	Left side oriented	Right side oriented
1^{st} (Point A)	$(x_s,\ z_s)$	$(x_s,\ z_s)$
2^{nd} (Point B)	$(x_d,\ z_d)$	$(x_d,\ z_d)$
3^{rd}	$(-\infty,\ z_d)$	$(\infty,\ z_d)$
4^{th}	$(-\infty,\ z_s)$	$(\infty,\ z_s)$

2.2 Inverse Modelling

Inverse modelling in geophysics is an optimization process for estimating geophysical parameters of underneath geological structures by minimizing misfit error between observed and estimated field data. Various optimization algorithms can invert such geophysical data in a more or less intelligent and efficient way. In general, geophysical inverse problems are non-unique, i.e. minimum misfit error can be found for different sets of optimizing parameters. In other words, different geological structures can provide the same observed field data. By incorporating any prior information about the parameters can reduce such non-uniqueness. The apriori pieces of information are fused into optimization algorithms as a constraint to invert the observed data for getting unique structures.

In our present study, the aim is to optimize listric fault structure by inverting observed gravity anomalies. The curvature of the listric fault plane can be expressed using quadratic Bezier curves. The weights of control points are the only parameters to represent the curved fault plane. There are six control points required to parametrize a 2D listric fault plane, and the corresponding weights are used as a model parameter in our optimization problems. By further constraining one control point, five model parameters are sufficient to invert the observed gravity anomalies to optimize any listric fault structure. The details of implementing constraints are discussed in the preceding section.

Optimization algorithms are the main building blocks for an inverse problem. Nowadays, swarm-based algorithms are popular in various science and engineering disciplines due to their robustness and flexibility. These are mainly global optimization algorithms inspired by the mass behaviour of social animals, suitable for a multi-dimensional real-valued optimization problem. PSO is one of the most potent meta-heuristic numerical global optimization algorithms applied in many fields due to its flexibility and simplicity. PSO was first introduced by Eberhart and Kennedy (1995), and it is inspired by the cumulative social behaviour of animals like a school of fishes or flock of birds. Our present study uses PSO as an optimization algorithm for inverting observed gravity anomalies for estimating listric fault structures. PSO is straightforward to implement, and it is independent of initial parameter selection. A detailed scheme (Marini & Walczak, 2015) of the basic PSO algorithm is shown in figure 3.

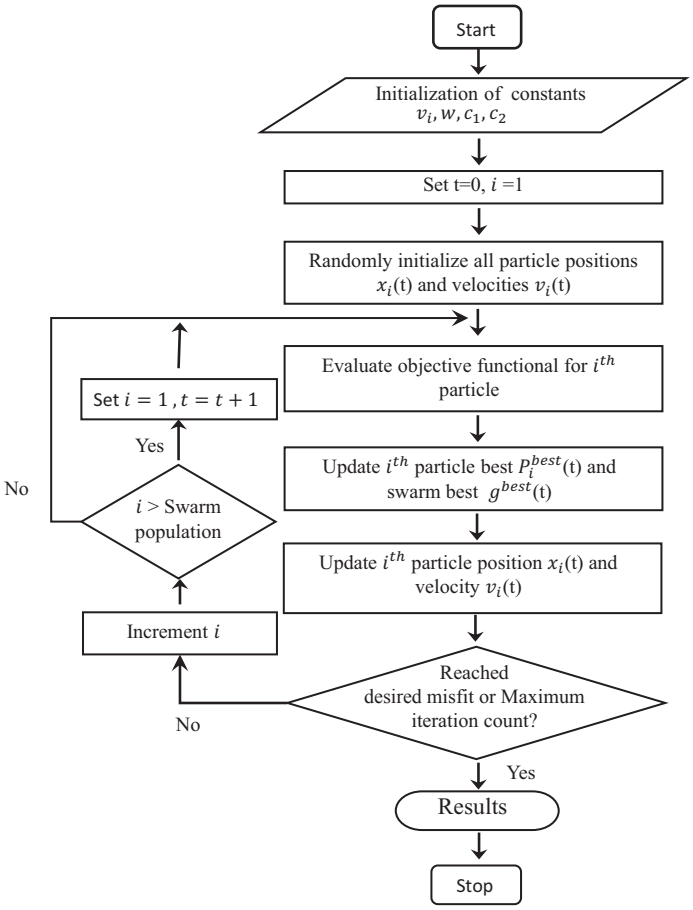

Figure 3. Scheme of the basic PSO algorithm.

Let us assume $f_z(x_j, z_j)$ is the observed gravity anomaly and $g_z(x_j, z_j)$ is the predicted gravity anomaly at any observed point (x_j, z_j) due to some model parameter $\mathrm{X_i}$. Then the objective function can be written as

$$Q = \sum_{i=1}^{k} (f_z(x_j, z_j) - g_z(x_j, z_j))^2. \tag{4}$$

Where k is the number of observation points, let us assume S is a D-dimensional search space for optimizing the objective function. In PSO, each candidate solution is known as 'particle', and each particle consists of D number of parameters that have to be optimized. At any time step t, the $\mathrm{i^{th}}$ particle can be represented as a vector $\mathrm{X_i(t)}$ in the search space as

$$\mathrm{X_i(t) = [x_{i1},\ x_{i2},\ x_{i3},\ \ldots,\ x_{iD}],\ where\ i \in \{1, 2, 3, \ldots, N\}} \tag{5}$$

and the swarm consist of N particles having dimension D. During the optimization process, the position of each particle updates for two consecutive time steps and follows the relation

$$\mathrm{X_i(t+1) = X_i(t) + V_i(t+1).} \tag{6}$$

Where $\mathrm{V_i(t+1)}$ is the velocity component of $\mathrm{i^{th}}$ particle at time step t + 1. The velocity component also updates as follow

$$\mathrm{V_i(t+1) = } w\mathrm{V_i(t)} + c_1 r_1 (\mathrm{P_i^{best}(t) - V_i(t)}) + c_2 r_2 (\mathrm{g^{best}(t) - V_i(t)}). \tag{7}$$

Where c_1, c_2 are real valued constant term named acceleration coefficients and r_1, r_2 are uniformly distributed random numbers having range [0,1]. $\mathrm{P_i^{best}(t)}$ is the parameters of best solution ever obtained by $\mathrm{i^{th}}$ particle termed as personal best and $\mathrm{g^{best}(t)}$ is the parameters of best solution obtained by entire swarm as known as global best. The term $w\mathrm{V_i(t)}$ is named inertia term and $c_1 r_1 (\mathrm{P_i^{best}(t) - V_i(t)})$, $c_2 r_2 (\mathrm{g^{best}(t) - V_i(t)})$ are termed as cognitive component and social component respectively. Usually the range for c_1, c_2 varies from $[0 < c_1, c_2 < 2]$ during the selection and a detailed parameter tuning is required for faster convergence of model parameters. A criterion for stable convergence developed by Perez and Behdinan (2007) are as follows

$$0 < c_1 + c_2 < 4, \tag{8}$$

$$\left(\frac{c_1 + c_2}{2} - 1\right) < w < 1. \tag{9}$$

The inertia coefficient (w) plays an important role to bypass uncontrolled velocity that can cause the divergence of the optimization problem. A perfect balance between exploration and exploitation is much needed for any global optimization problem. By tuning the inertia term, velocity modulation can be controlled. For larger inertia weight, it facilitates global search that covers the entire search space, where smaller inertia weight assists local exploitation. A higher value of inertia weight is always desirable during initial iterations,

followed by smaller inertia weight at maximum iterations. An effective arrangement for the steady reduction of inertia weight is desirable for optimization. In this direction Shi and Eberhart (1998) used random inertia weight, Arumugam and Rao (2006) used global-local best inertial weight, Y. Feng et al. (2007) developed chaotic descendent inertia weight, etc. In our present study, a linearly decreasing inertia weight proposed by Xin et al. (2009) is used for the optimization problem. The dynamic adjustment strategies become

$$w_t = w_{max} - \left(\frac{w_{max} - w_{min}}{t_{max}}\right) \times t, \tag{10}$$

where $w(t)$ is the inertia weight at t^{th} time step. w_{max} and w_{min} are the maximum and minimum range of w that can be obtained from acceleration coefficients shown in equation 9. t_{max} is the maximum time step for the optimization algorithm.

2.3 Bezier curves and cost function

Bezier curve was first introduced by French engineer Pierre Bezier for designing the bodywork of automobiles. Bezier curves have many applications in science, engineering designing, computer-aided design systems, animation, robotics, networks, etc. The main advantage of Bezier curves is that they are computationally simple and stable. The mathematical descriptions are compact, intuitive and elegant. It is easy to compute and able to represent any shape of a curve. The mathematical basis for Bezier curves is the Bernstein polynomials. The basis vectors are summed up with the help of some set of control points to represent any curve. The Bezier curve can be expressed mathematically as

$$z(t) = \sum_{i=0}^{n} P_i B_i^n(t), \tag{11}$$

where P_i are the set of control points and $B_i^n(t)$ are the Bernstein polynomials. The Bernstein polynomials are represented as

$$B_i^n(t) = \binom{n}{i}(1-t)^{n-i}t^i, \ for\ 0 < t < 1. \tag{12}$$

Where n is the degree of the polynomial. For any quadratic Bezier curve, three control points are required, and the path traced by the function $Z(t)$ can be written as

$$Z(t) = (1-t)[(1-t)P_0 + tP_1] + t[(1-t)P_1 + tP_2], \ for\ 0 < t < 1. \tag{13}$$

In our present study, the listric fault plane can be represented by a quadratic Bezier curve for lessening the parameters for optimization. The listric fault lies in a 2D plane; hence, each control point's dimension is also two for representing the fault plane. That implies, in total, six parameters are required to be optimized. The first and last control points are always the endpoints of the curve for any Bezier curves. As the shallower vertex of the fault is lying on the surface, we can be constraining the vertical position of the first point that can reduce one parameter. Hence the number of actual parameters is five to optimize the fault plane. The gravity anomaly due to the parametrized fault plane can be obtained from the line integral (equation 3). Let us assume the operator $\hat{\chi}$ can evaluate the gravity anomaly due to the fault plane parametrized by the Bezier curve. Hence the cost function for the optimization problem can be written as

$$
\begin{aligned}
Q &= \sum_{i=1}^{n} (f_z(x_j, z_j) - g_z(x_j, z_j))^2 \\
&= \sum_{i=1}^{n} (f_z(x_j, z_j) - \hat{\chi}(Z(t_i)))^2 \\
&= \sum_{i=1}^{n} (f_z(x_j, z_j) - \hat{\chi}(\sum_{j=0}^{k} P_j B_j^k(t_i)))^2. \qquad (14)
\end{aligned}
$$

Hence the cost function only depends on control point parameters P_j of the quadratic Bezier curve. PSO is used here for optimizing the cost function, and the optimized parameters are further used to reconstruct the listric fault plane. Few synthetic models, a detailed uncertainty appraisal and application of real listric fault is discussed in detail in the preceding section.

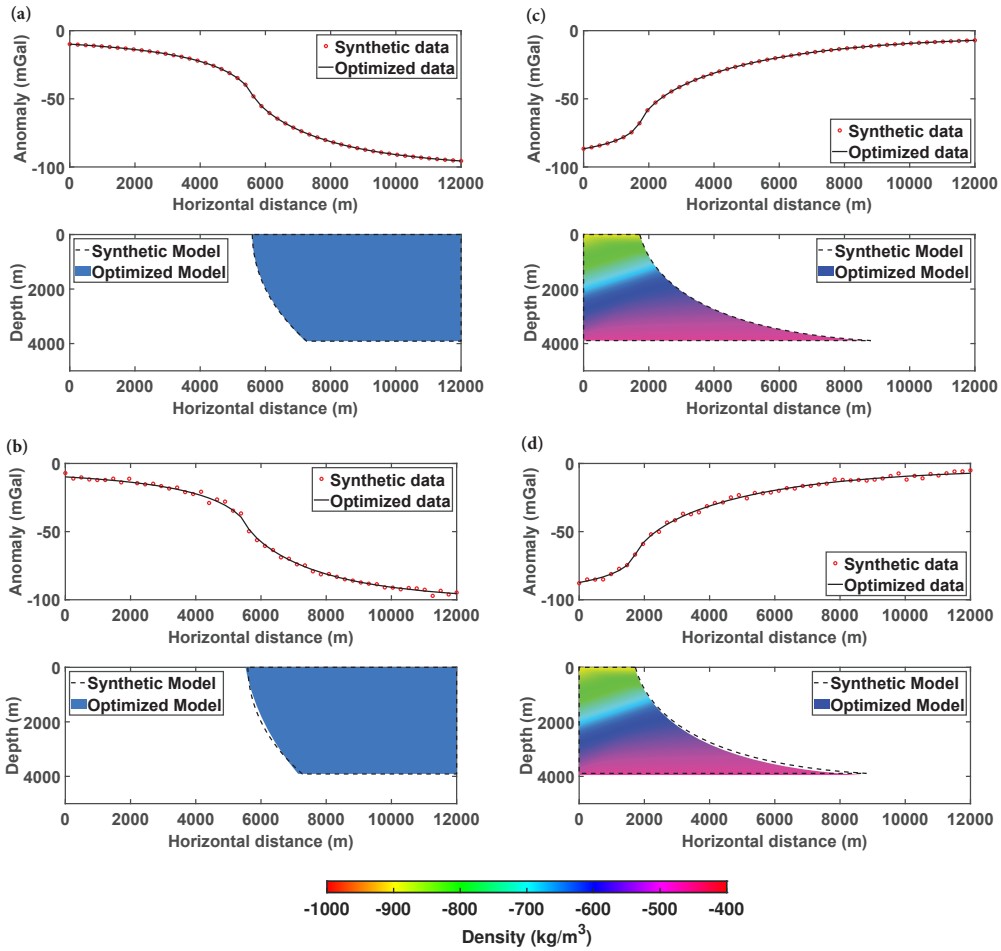

Figure 4. Inverted listric fault structure from synthetic gravity anomalies for (a) Model 1 without noise, (b) Model 1 with noise, (c) Model 2 without noise, and (d) Model 2 with noise. The synthetic gravity anomalies are denoted with the red dotted curve, and the optimized anomalies are shown in the upper panel denoted as the solid blue line. The inverted fault structures are represented as filled regions, and the actual structures are denoted by the black dashed line.

3 Results

In this section, the application of the developed algorithm is performed for various synthetic and real models. PSO is used here as an optimization algorithm, and all control parameters of PSO are tunned for faster convergence of model parameters. Two different types of density distributions, (1) uniform density contrast and (2) depth varying density contrast, are applied to evaluate the versatility of the algorithm. Further, all synthetic models are contaminated with white Gaussian noise to check the algorithm robustness.

3.1 Synthetic Models

Gravity anomalies for two different synthetic fault structures are inverted using the developed algorithms having predefined density distributions. A normal listric fault with fixed density distribution is defined as model 1, and model 2 consists of reverse listric fault with exponential density distributions shown in figure 4. The gravity anomalies for models 1 and 2 are further contaminated with Gaussian noise having a mean of 0 mGal and a standard deviation of 1.5 mGal. The profile length for gravity anomalies for both the models is around 12 km long with a maximum depth of 3.9 km for model 1 and 3.8 km for model 2. In total, 50 equidistant data points are considered for the inversion of gravity anomalies. We have considered a uniform density distribution for model 1, with a density contrast of -650 kg/m^3 and exponential depth varying density distribution for model 2. The density contrast for model 2 is

$$\Delta\rho(z) = (-0.40 - 0.5 \times exp(-0.5 \times z \times 10^{-3})) \times 1000 \qquad \text{kg/m}^3. \tag{15}$$

Our algorithm is versatile enough to invert any mathematical form of depth varying density distribution regardless of uniform and exponential density contrast.

Table 2. Comparison for both the models in terms of depth, Frechet distance and rms error of gravity anomaly.

Model type	Depth (m)	Frechet distance (m)	rms error (mGal)
Model 1 true	3912.10	-	-
Model 1 inverted noise free	3911.72	66.99	2.81×10^{-3}
Model 1 inverted with noise	3898.80	360.92	1.98×10^{0}
Model 2 true	3891.02	-	-
Model 2 inverted noise free	3891.41	69.51	9.57×10^{-3}
Model 2 inverted with noise	3890.65	550.60	3.03×10^{0}

In PSO algorithm, the control parameters are acceleration coefficients (c_1, c_2), total population of the swarm (nPoP) and inertia weight(w). The inertia weights are dynamically adjustable and linearly varying as shown in equation 10. The swarm population plays a pivotal role in the convergence speed. By increasing the swarm population, convergence is achieved in lesser iterations by broadening the computational time. Hence a perfect balance between convergence speed and iteration counts are required for an inexpensive model. Similarly, the acceleration coefficients are also varying from a range [0, 2]. A detailed parameter tuning is required for faster converging and accurate parameter optimization. In this direction, both the models run for a nPoP range [0, 100], acceleration coefficient range of [0, 2] with a maximum time step of 1000 and relative misfit cut-off of an order of 10^{-3}. In

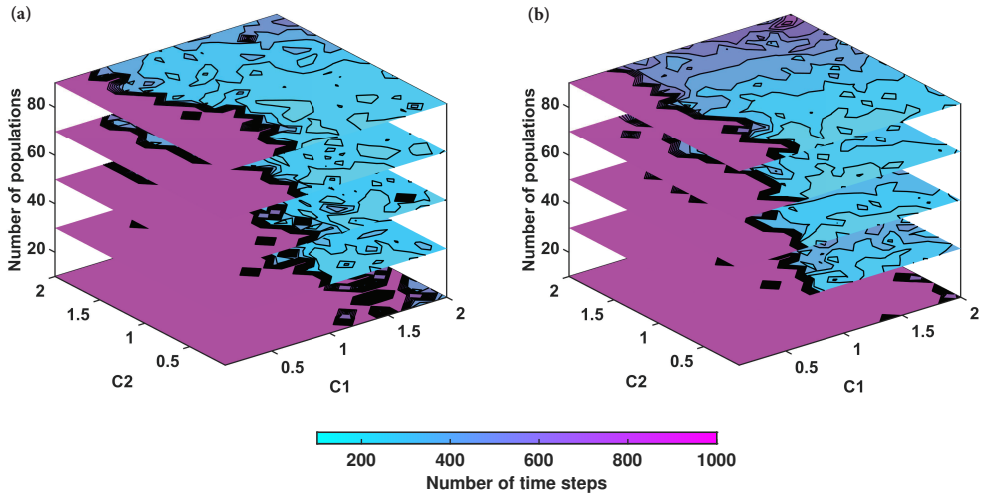

Figure 5. Parameter tuning for acceleration coefficients (c_1, c_2) and swarm population (nPoP) in terms of time steps for (a) Model-1 and (b) Model-2.

figure 5, a detailed stack plot for number of iteration count for various range of nPoP, c_1 and c_2 are shown. It can be observed that for nPoP greater 20, and acceleration coefficient range $1.4 < c_1 < 2.0$ and $0.2 < c_2 < 2.0$, both the models converge with minimum iteration count. The time range also varies for [10, 20] seconds by increasing the population count. Hence in our presented algorithm we choose the nPoP =40, c_1=1.4 and c_2=1.7 as an optimal choice of control parameter for any synthetic and real data inversion.

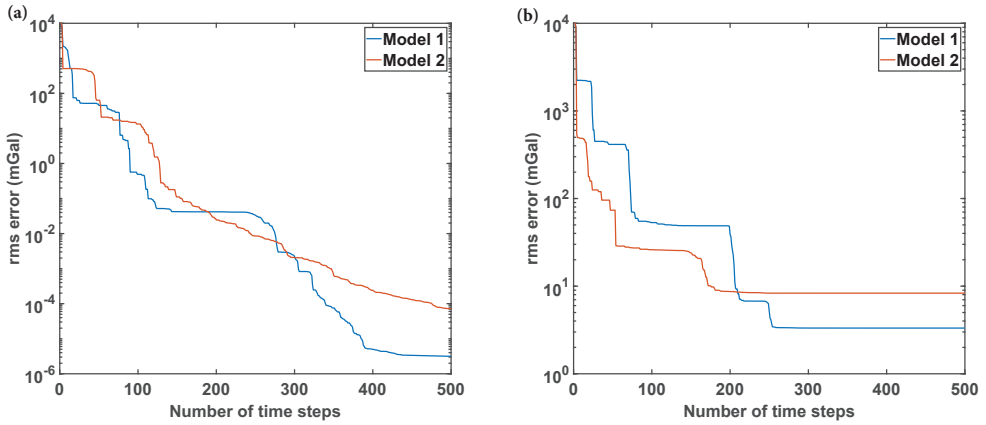

Figure 6. rms error plot of actual and inverted gravity anomalies with respect to time steps for (a) Model-1 and (b) Model-2.

After selecting the control parameters for PSO, the gravity anomalies for both the models are inverted and compare with the true structures of synthetic listric faults as shown in figure 4. Both the gravity anomalies are incorporated with noise, and the noisy data are inverted to check the robustness of the presented scheme. A detailed comparison for true model and inverted model for both noisy and noise-free data are shown in table 2. Here

we use Frechet distance to measure the deviation of fault planes from true models and inverted models. Frechet distances are utilized for the measuring of similarities between irregular curves. It is generally used to measure the similarities between trajectories of moving objects. Here we have used it as a performance parameter of our model to check the algorithm's accuracy. The higher value of Frechet distance indicating more dissimilarities of the model and vice versa. In the optimization process for each model, five independent model runs are performed for maximum time steps of 500. The minimum misfit error out of all independent runs is considered the best-inverted model, and the corresponding model parameters are used to reconstruct the fault plane. Finally, the rms error in each time step is plotted for noisy and noise-free models as shown in figure 6. It can be observed that the minimum misfit error for noise-free models are the order of 10^{-7} and for noisy data is 10^{-2} for both the model configurations. The convergence achieves before the maximum time step. Unlike the inversion of any other potential field problem, gravity inversion is also non-unique, and data acquisition is erroneous due to noise incorporation. Here we incorporated density distribution as a constraint to get a unique, optimized structure. However, a proper uncertainty appraisal is a pivotal step to access the reliability of the inverted structures. Fernández-Martínez et al. (2013); Pallero et al. (2015) applied an equivalent region approach using cost function topography in a 2D PCA plane to evaluate the uncertainty analysis. We also adopted the same technique for the uncertainty appraisal for both models. The misfit error between observed and inverted anomalies gradually decreases during the optimisation process, and the optimizing parameters converge to the true solution. An equivalent region is a 2D space where all solutions below some predefined relative misfit cutoff are preserved. The relative misfit between observed and inverted gravity anomaly can be defined as

$$\phi_{rel} = \frac{\|f_z - g_z\|_2}{\|f_z\|_2} \times 100. \tag{16}$$

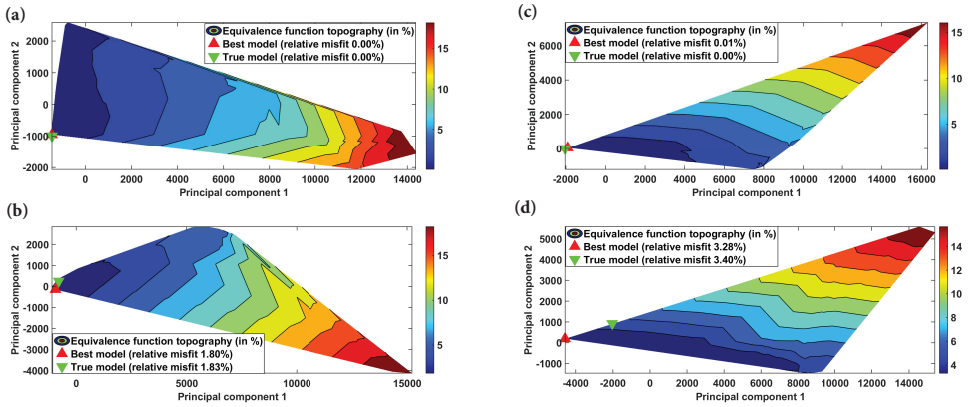

Figure 7. Equivalence function topography in 2D PCA plane for (a) Model 1 noise-free data, (b) Model 1 noise incorporated data, (c) Model 2 noise-free data, (d) Model 2 noise incorporated data.

In general, the cut off for relative misfit is 2-5 times the noise incorporation. Here for both the models, the minimum noise is around 5%, and the cutoff is considered as 25%. Let us assume $X = [S_1, S_2, \ldots S_q]$ are the solution set that satisfies the cutoff criterion. Each solution set consists of five parameters of Bezier curves control points that represent the listric fault plane. In the next step, a covariance matrix is constructed using the matrix formed by the solution set. Here X represents a matrix whose column vectors are the solution set, the covariance matrix having the form

$$C = (X - \mu)^T \cdot (X - \mu), \tag{17}$$

where μ is the mean of the solution set, the primary purpose of the covariance matrix is to find the eigenvectors and construct a PCA space to project all solutions and get a better visual representation. The first two eigenvectors corresponding to leading eigenvalues are known as principal components that form a 2D PCA space to represent the misfit error as a contour plot which is shown in figure 7 for both the models. All models are converged within a maximum iteration of 500. The parameters achieved in the last iteration of the algorithm are known as the best model, and the parameters for the actual synthetic model are known as the true model. When the gravity anomaly for all synthetic models are not contaminated with noise, the true model and best model coincides in the 2D PCA plane and located at the lowest misfit region. The true and best models are not coinciding for noisy data but are situated at the lowest misfit region. The relative misfit error for the true model is greater than the best-optimized model. These are the primary outcomes of uncertainty appraisal for the reliability of the inverted model.

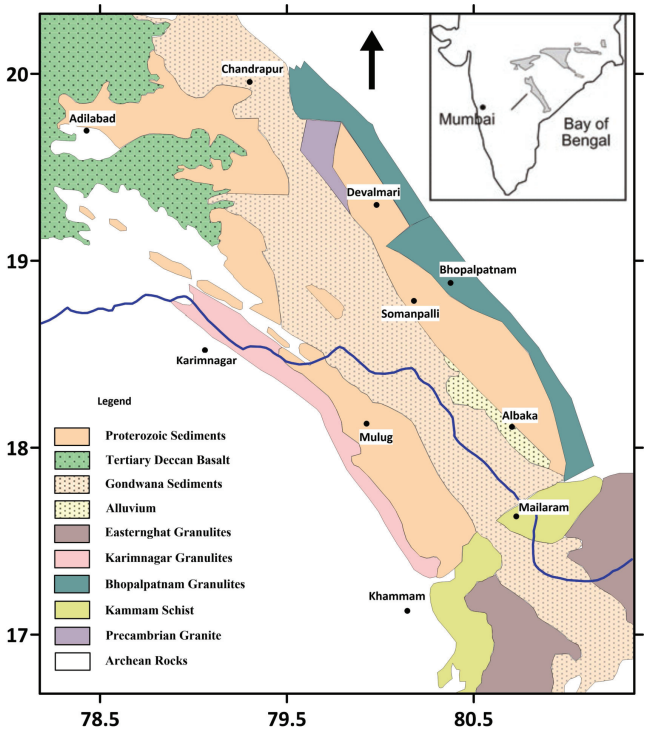

Figure 8. Geology map for Pranhita-Godavari valley obtained from Amarasinghe et al. (2014)

3.2 Real Model

In the previous section, different combinations of synthetic fault structures are inverted, providing an accurate, robust, and reliable solution from observed gravity anomalies. Here the optimization technique is applied to invert real gravity anomalies due to listric fault having depth varying density distribution from Godavari sub-basin. The sequences of Gondwana are obtained in the southern part of the Indian subcontinent. The NW-SE trending Pranhita-Godavari valley is one of the major repositories of the Gondwana successions. Pranhita-Godavari valley is further divided into four sub-basins such as Krishna-Godavari, Godavari, Chintalpudi and Kothagudem based on the nature of lithologic

sequences (Ramanamurthy & Parthasarathy, 1988). A detailed geology map is shown in figure 8. The northeastern side of the Godavari sub-basin is characterized by a half-graben structure named as Ahiri-Cherla master fault (Qureshy et al., 1968). Chakravarthi and Sundararajan (2004) inverted gravity anomalies to estimate a planner fault structure due to parabolic density distribution. Further Chakravarthi et al. (2017) inverted the observed gravity anomalies to estimate the listric fault plane using higher-order polynomials.

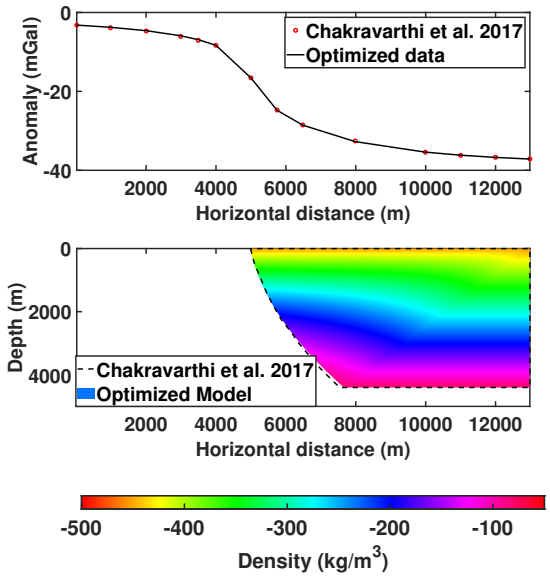

Figure 9. Inverted structure for Ahiri-Cherla master fault. The observed gravity anomalies are denoted with the red dotted curve, and the optimized anomalies are shown in the upper panel denoted as the solid blue line. The inverted fault structures are represented as filled regions, and the structure obtained by (Chakravarthi et al., 2017) are denoted by the black dashed line.

In our present study, the Bouguer anomaly throughout the Ahiri-Cherla master fault is inverted using the Bezier curve and compared the result obtained by Chakravarthi et al. (2017). The density contrast is obtained from borehole logging and fitted exponentially as follows

$$\Delta\rho(z) = (-0.4554 \times exp(-0.3929 \times z \times 10^{-3})) \times 1000 \qquad \text{kg/m}^3. \tag{18}$$

A rigorous gravity survey throughout the Godavari sub-basin was performed by Mishra et al. (1989). A 13 km long gravity anomaly profile was digitized from Chakravarthi and Sundararajan (2004); Chakravarthi et al. (2017) along the fault plane. The residual gravity anomaly is inverted using the presented algorithm, and the estimated structure is shown in figure 9. The Frechet distance between the inverted fault plane using the Bezier curve and using higher-order polynomial by Chakravarthi et al. (2017) are around 272.63 m. which indicates the good agreement with the structure estimation with the earlier work. The maximum depth is about 4404.85 m, and the rms error between observed and estimated gravity anomalies is 0.3705 mGal. Hence, the Bezier curve optimized model is less parametrized and accurately estimates the listric fault plane for a real scenario.

4 Graphical User Interface

A compact and user-friendly Matlab based graphical user interface named 'ListricFaultInv' is developed to estimate the underneath listric fault structure due to any depth varying density distribution from observed gravity anomalies. Any prerequisite knowledge of programming language or detailed understanding of the present algorithm is not needed to estimate fault structure from observed gravity anomalies. The GUI popped up by running the Matlab file 'ListricFaultInv.m', and it is auto adjustable as per the screen resolution shown in figure 10. Two ASCII text files containing the gravity anomaly and corresponding observation points are required for the optimization. Gravity anomalies must have to be in the mGal unit, and observation points are in meters. Two dedicated browser buttons are provided for importing the data. The functional form of depth varying density distribution are also required as model input parameters.

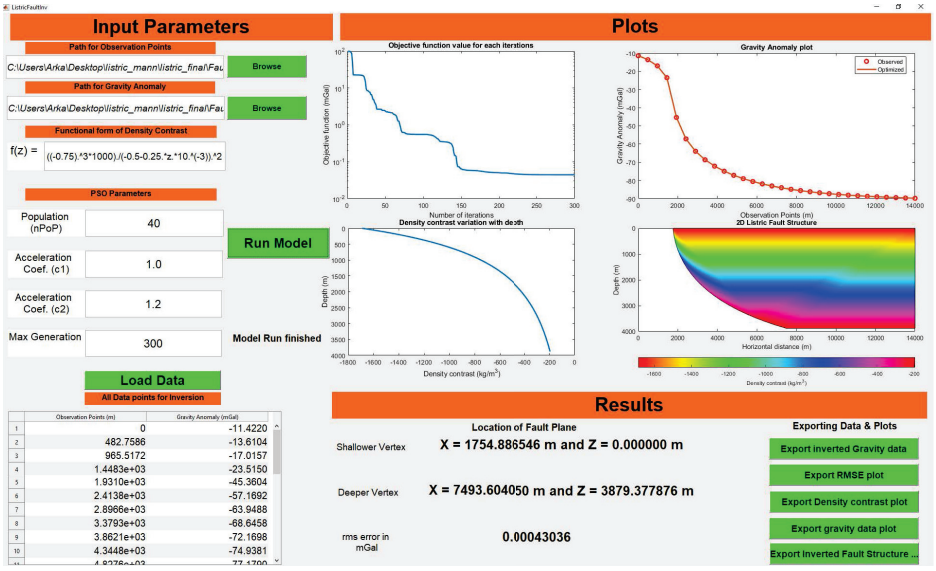

Figure 10. The user interface of ListricFaultInv GUI.

Although the control parameters of PSO algorithm are tuned initially, in this GUI, any user can change the control parameters as per their choice. Finally, a push-button named 'load data' is provided for showcasing the observed anomalies at different observation points in a separate tabular format. Only this information is needed to run the model for structural estimation. Finally, by clicking the 'run model' button, four plots are generated at the end of the optimization problem. The plots are listric fault structure, observed and inverted gravity anomaly, objective function value after each iteration and the depth varying density contrast plot. All optimized data and plots can be exported in any existing file format. The location of the shallower and the deeper vertex of the fault plane, the rms error of observed, and inverted gravity anomalies can be shown in the result section.

5 Conclusion

In this paper, our primary motivation is to provide some insight to develop a unified algorithm for inverting gravity anomalies due to any listric fault structures. A detailed uncertainty appraisal is performed in different synthetic models for the reliability of the algorithm. The versatility of the algorithm is that it can invert gravity anomalies due to any depth varying density distributions. Furthermore, no prior model selection is required due to the usage of global optimization. It is the first time representing the fault plane in terms

of the Bezier curve by adjusting the control points. It also required a fixed number of model parameters to reconstruct any complicated structures. Finally, a graphical user interface is designed to visualize any fault structure reconstruction without any computational difficulties. The presented algorithm is demonstrated for real fault structure estimation from the Godavari sub-basin, and the obtained structure provides good agreement with previously published literature.

6 Data Availability Statement

All computational codes and synthetic data can be obtained from Github public repository link `https://github.com/ArkaRoy-Matlab/ListricFault` . The observed gravity anomaly data for real listric fault structure is digitized from the paper [Chakravarthi, V., Kumar, M. P., Ramamma, B., & Sastry, S. R. (2017). Gravity anomaly interpretation of 2D fault morphologies by means of nonplanar fault planes and exponential density contrast model: a space domain technique. Arabian Journal of Geosciences, 10(3), 64].

Acknowledgments

We thank the Director, NCESS, and the Secretary, MoES, Government of India, for providing funds and unconditional support to carry out this work. We are also thankful to the former Director of NCESS, P. C. Rao, and the deputy group head, J. K. Tomsom, who imparted thoughtful suggestions. We thank Nilanjana Sorcar for her helpful discussions.

References

Abdelrahman, E., & Essa, K. (2015). Three least-squares minimization approaches to interpret gravity data due to dipping faults. Pure and Applied Geophysics, 172(2), 427–438.

Alatorre-Zamora, M.-A., & Campos-Enriquez, J.-O. (1991). La primavera caldera (mexico): structure inferred from gravity and hydrogeological considerations. Geophysics, 56(7), 992–1002.

Amarasinghe, U., Chaudhuri, A., Collins, A., Deb, G., & Patranabis-Deb, S. (2014, 04). Evolving provenance in the proterozoic pranhita-godavari basin, india. Geoscience Frontiers, 6. doi: 10.1016/j.gsf.2014.03.009

Arumugam, M. S., & Rao, M. (2006). On the performance of the particle swarm optimization algorithm with various inertia weight variants for computing optimal control of a class of hybrid systems. Discrete Dynamics in Nature and Society, 2006.

Bally, A., Bernoulli, D., Davies, G., & Montadert, L. (1981). Listric normal faults. Oceanologica Acta, Special issue.

Biswas, A. (2015). Interpretation of residual gravity anomaly caused by simple shaped bodies using very fast simulated annealing global optimization. Geoscience Frontiers, 6(6), 875–893.

Chakravarthi, V. (2010). Gravity anomalies of 2d fault structures with fault planes described by polynomial functions of arbitrary degree. Current Science (00113891), 99(5).

Chakravarthi, V. (2011). Automatic gravity optimization of 2.5 d strike listric fault sources with analytically defined fault planes and depth-dependent density. Geophysics, 76(2), I21–I31.

Chakravarthi, V., Kumar, M. P., Ramamma, B., & Sastry, S. R. (2017). Gravity anomaly interpretation of 2d fault morphologies by means of nonplanar fault planes and exponential density contrast model: a space domain technique. Arabian Journal of Geosciences, 10(3), 64.

Chakravarthi, V., & Sundararajan, N. (2004). Ridge-regression algorithm for gravity inversion of fault structures with variable density. Geophysics, 69(6), 1394–1404.

Chakravarthi, V., & Sundararajan, N. (2007a). 3d gravity inversion of basement relief—a depth-dependent density approach. Geophysics, 72(2), I23–I32.

Chakravarthi, V., & Sundararajan, N. (2007b). Marquardt optimization of gravity anomalies of anticlinal and synclinal structures with prescribed depth-dependent density. Geophysical prospecting, 55(4), 571–587.

Crossley, D. J., & Clarke, G. K. (1970). Gravity measurements on "fox glacier", yukon territory, canada. Journal of Glaciology, 9(57), 363–374.

Eberhart, R., & Kennedy, J. (1995). A new optimizer using particle swarm theory. In Mhs'95. proceedings of the sixth international symposium on micro machine and human science (pp. 39–43).

Ekinci, Y. L., Balkaya, Ç., Göktürkler, G., & Turan, S. (2016). Model parameter estimations from residual gravity anomalies due to simple-shaped sources using differential evolution algorithm. Journal of Applied Geophysics, 129, 133–147.

Elhussein, M. (2021). New inversion approach for interpreting gravity data caused by dipping faults. Earth and Space Science, 8(2), e2020EA001075.

Essa, K. S. (2013). Gravity interpretation of dipping faults using the variance analysis method. Journal of Geophysics and Engineering, 10(1), 015003.

Essa, K. S., & Munschy, M. (2019). Gravity data interpretation using the particle swarm optimisation method with application to mineral exploration. Journal of Earth System Science, 128(5), 1–16.

Feng, X., Wang, W., & Yuan, B. (2018). 3d gravity inversion of basement relief for a rift basin based on combined multinorm and normalized vertical derivative of the total horizontal derivative techniques. Geophysics, 83(5), G107–G118.

Feng, Y., Teng, G.-F., Wang, A.-X., & Yao, Y.-M. (2007). Chaotic inertia weight in particle swarm optimization. In Second international conference on innovative computing, informatio and control (icicic 2007) (pp. 475–475).

Fernández-Martínez, J. L., Fernández-Muñiz, Z., Pallero, J., & Pedruelo-González, L. M. (2013). From bayes to tarantola: New insights to understand uncertainty in inverse problems. Journal of Applied Geophysics, 98, 62–72.

Florio, G. (2020). The estimation of depth to basement under sedimentary basins from gravity data: Review of approaches and the itresc method, with an application to the yucca flat basin (nevada). Surveys in Geophysics, 41(5), 935–961.

Güntner, A., Schmidt, R., & Döll, P. (2007). Supporting large-scale hydrogeological monitoring and modelling by time-variable gravity data. Hydrogeology Journal, 15(1), 167–170.

Jaffal, M., El Goumi, N., Kchikach, A., Aïfa, T., Khattach, D., & Manar, A. (2010). Gravity and magnetic investigations in the haouz basin, morocco. interpretation and mining implications. Journal of African Earth Sciences, 58(2), 331–340.

Li, W., Liu, Y., Li, B., & Luo, F. (2016). Hydrocarbon exploration in the south yellow sea based on airborne gravity, china. Journal of Earth Science, 27(4), 686–698.

Li, Y., & Oldenburg, D. W. (1996). 3-d inversion of magnetic data. Geophysics, 61(2), 394–408.

Marini, F., & Walczak, B. (2015). Particle swarm optimization (pso). a tutorial. Chemometrics and Intelligent Laboratory Systems, 149, 153–165.

Mishra, D., Gupta, S., & Venkatarayudu, M. (1989). Godavari rift and its extension towards the east coast of india. Earth and Planetary Science Letters, 94(3-4), 344–352.

Montesinos, F., Arnoso, J., & Vieira, R. (2005). Using a genetic algorithm for 3-d inversion of gravity data in fuerteventura (canary islands). International Journal of Earth Sciences, 94(2), 301–316.

Nagihara, S., & Hall, S. A. (2001). Three-dimensional gravity inversion using simulated annealing: Constraints on the diapiric roots of allochthonous salt structures. Geophysics, 66(5), 1438–1449.

Pallero, J., Fernandez-Martinez, J. L., Bonvalot, S., & Fudym, O. (2015). Gravity inversion and uncertainty assessment of basement relief via particle swarm optimization. Journal of Applied Geophysics, 116, 180–191.

Perez, R. l., & Behdinan, K. (2007). Particle swarm approach for structural design optimization. Computers & Structures, 85(19-20), 1579–1588.

Portniaguine, O., & Zhdanov, M. S. (2002). 3-d magnetic inversion with data compression and image focusing. Geophysics, 67(5), 1532–1541.

Qin, P., Huang, D., Yuan, Y., Geng, M., & Liu, J. (2016). Integrated gravity and gravity gradient 3d inversion using the non-linear conjugate gradient. Journal of Applied Geophysics, 126, 52–73.

Qureshy, M., Brahmam, N. K., Garde, S., & Mathur, B. (1968). Gravity anomalies and the godavari rift, india. Geological Society of America Bulletin, 79(9), 1221–1230.

Ramanamurthy, B., & Parthasarathy, E. (1988). On the evolution of the godavari gondwana graben, based on landsat imagery interpretation. Journal of Geological Society of India (Online archive from Vol 1 to Vol 78), 32(5), 417–425.

Rose, M., Zeng, Y., & Dransfield, M. (2006). Applying falcon® gravity gradiometry to hydrocarbon exploration in the gippsland basin, victoria. Exploration Geophysics, 37(2), 180–190.

Roy, A., Dubey, C. P., & Prasad, M. (2021a). Gravity inversion for heterogeneous sedimentary basin with b-spline polynomial approximation using differential evolution algorithm. Geophysics, 86(3), F35–F47.

Roy, A., Dubey, C. P., & Prasad, M. (2021b). Gravity inversion of basement relief using particle swarm optimization by automated parameter selection of fourier coefficients. Computers & Geosciences, 156, 104875.

Roy, A., & Kumar, T. S. (2021). Gravity inversion of 2d fault having variable density contrast using particle swarm optimization. Geophysical Prospecting, 69(6), 1358–1374.

Roy, L., Agarwal, B., & Shaw, R. (2000). A new concept in euler deconvolution of isolated gravity anomalies. Geophysical prospecting, 48(3), 559–576.

Shelton, J. W. (1984). Listric normal faults: an illustrated summary. AAPG Bulletin, 68(7), 801–815.

Sheth, H. (1998). A reappraisal of the coastal panvel flexure, deccan traps, as a listric-fault-controlled reverse drag structure. Tectonophysics, 294(1-2), 143–149.

Shi, Y., & Eberhart, R. (1998). A modified particle swarm optimizer. In 1998 ieee international conference on evolutionary computation proceedings. ieee world congress on computational intelligence (cat. no. 98th8360) (pp. 69–73).

Silva, J., Costa, D. C., & Barbosa, V. C. (2006). Gravity inversion of basement relief and estimation of density contrast variation with depth. Geophysics, 71(5), J51–J58.

Silva, J., Santos, D., & Gomes, K. (2014). Fast basement relief inversion. Geophysics, 79(5), G79–G91.

Song, M., Yi, P., Xu, J., Cui, S., Shen, K., Jiang, H., ... Wang, H. (2012). A step metallogenetic model for gold deposits in the northwestern shandong peninsula, china. Science China Earth Sciences, 55(6), 940–948.

Srivastava, S., Datta, D., Agarwal, B., & Mehta, S. (2014). Applications of ant colony optimization in determination of source parameters from total gradient of potential fields. Near Surface Geophysics, 12(3), 373–390.

Suess, E. (1909). The face of the earth: Das antlitz der erde (Vol. 4). Clarendon Press.

Talwani, M., Worzel, J. L., & Landisman, M. (1959). Rapid gravity computations for two-dimensional bodies with application to the mendocino submarine fracture zone. Journal of geophysical research, 64(1), 49–59.

Tinto, K., & Bell, R. E. (2011). Progressive unpinning of thwaites glacier from newly identified offshore ridge: Constraints from aerogravity. Geophysical Research Letters, 38(20).

Toushmalani, R. (2013). Gravity inversion of a fault by particle swarm optimization (pso). SpringerPlus, 2(1), 1–7.

Veiga, M. M., & Gunson, A. J. (2020). Gravity concentration in artisanal gold mining. Minerals, 10(11), 1026.

Wan, L., & Zhang, J. (2019). Analytical solutions of gravity vector and gravity gradient tensor caused by a 2d polygonal body with a 2d polynomial density contrast. Surveys in Geophysics, 1–33.

Winckel, G. V. (2004). Legendre-gauss quadrature weights and nodes. MATLAB Central File Exchange, (https://www.mathworks.com/matlabcentral/fileexchange/4540-legendre-gauss-quadrature-weights-and-nodes).

Xin, J., Chen, G., & Hai, Y. (2009). A particle swarm optimizer with multi-stage linearly-decreasing inertia weight. In 2009 international joint conference on computational sciences and optimization (Vol. 1, pp. 505–508).

Yamada, Y., & McClay, K. (2003). Application of geometric models to inverted listric fault systems in sandbox experiments. paper 1: 2d hanging wall deformation and section restoration. Journal of structural geology, 25(9), 1551–1560.

Zhang, J., Wang, C.-Y., Shi, Y., Cai, Y., Chi, W.-C., Dreger, D., ... Yuan, Y.-H. (2004). Three-dimensional crustal structure in central taiwan from gravity inversion with a parallel genetic algorithm. Geophysics, 69(4), 917–924.

Zhou, X. (2008). 2d vector gravity potential and line integrals for the gravity anomaly caused by a 2d mass of depth-dependent density contrast. Geophysics, 73(6), I43–I50.

Zhou, X. (2009). General line integrals for gravity anomalies of irregular 2d masses with horizontally and vertically dependent density contrast. Geophysics, 74(2), I1–I7.

Zhou, X. (2013). Gravity inversion of 2d bedrock topography for heterogeneous sedimentary basins based on line integral and maximum difference reduction methods. Geophysical Prospecting, 61(1), 220–234.